Supporting Information

Wang et al. 10.1073/pnas.0913001107

SI Methods

Whole-Cell Voltage-Clamp Recording. Experiments were performed at room temperature. Fire-polished patch pipettes were made from 1.28-mm borosilicate capillary glass (Warner Instruments) with a tip resistance of 1–2 MΩ. Tight seals (>1 GΩ) were obtained before breaking into the whole-cell mode. The series resistance during recording varied from 5–10 MΩ and was not compensated. The pipette and bath solutions contained 140 mM *N*-methyl-D-glucamine chloride, 1 mM $MgCl_2$, 3 mM EGTA, and 5 mM Hepes (pH 7.4 with HCl). MgATP (2 mM) was added to the pipette solution. Current records were low-pass-filtered (2 kHz; Bessel; four-pole filter, −3 dB), digitized (20 kHz, 16-bit resolution), and stored on computer disk for later analysis using pCLAMP 8 software (Axon Instruments). A voltage ramp protocol was used (±80 mV). The net CFTR current was calculated as the difference in current between +80 and 0 mV after bath application of a mixture of 10 μM forskolin, 100 μM 3-isobutyl-1-methylxanthine, and 40 μM 8-(4-chlorophenylthio)-cAMP and subtraction of the current remaining after addition of a CFTR inhibitor (400 μM glibenclamide). Whole-cell capacitance was obtained from the amplifier after the compensation of the capacitative current. The mean current density was calculated as the ratio of the net whole-cell current and cell capacitance (pA/pF).

Surface Biotinylation and Immunoprecipitations. Cell surface proteins were biotinylated for 30 min at 4 °C with EZ-Link Sulfo-NHS-SS-Biotin (Pierce) (1 mg/mL) in PBS (pH 8.0) or with PBS only (control experiment). After the biotinylation step, the excess biotin was neutralized by incubating cells for 10 min at 4 °C with 1% BSA in PBS. Cells were then rinsed with PBS and incubated with or without 100 mM 2-mercaptoethanesulfonic acid (MESNA) in 50 mM Tris, 100 mM NaCl, 1 mM EDTA, 0.2% BSA, pH 8.6. After the MESNA stripping step, the excess MESNA was neutralized by incubating cells for 10 min at 4 °C with 1% BSA in PBS. Biotinylated cells were lysed in 1% Triton X-100 in PBS with protease inhibitors (complete, EDTA-free; Roche Applied Science) (1 mL per dish), and cell lysates were cleared by centrifugation (16,000 × *g* for 15 min at 4 °C). The total protein content of supernatants was determined by the MicroBCA protein assay kit (Pierce). Ten milligrams of total protein from each sample was incubated with streptavidin beads (streptavidin-agarose; Novagen) to isolate cell surface proteins, and 1 mg of total protein was immunoprecipitated with an anti-CFTR C-terminus antibody (24-1 monoclonal antibody; R&D Systems) cross-linked to A/G agarose beads to determine total CFTR expression. Streptavidin pull-downs and immunoprecipitations were carried out overnight at 4 °C. The beads were then rinsed three times with 1% Triton X-100 in PBS, and proteins were eluted by incubation at 37 °C for 30 min with reducing Laemmli buffer (plus 50 mM DTT, 1.2 (v/v) β-mercaptoethanol). After a brief centrifugation (1 min, 3,000 × *g*), proteins in the supernatants were resolved by SDS/PAGE on a 4–15 (w/v) acrylamide gel and then transferred to PVDF membrane. Blots were performed with the anti-CFTR C-terminus antibody described previously (1).

1. Wang W, et al. (2005) Reversible silencing of CFTR chloride channels by glutathionylation. *J Gen Physiol* 125:127–141.

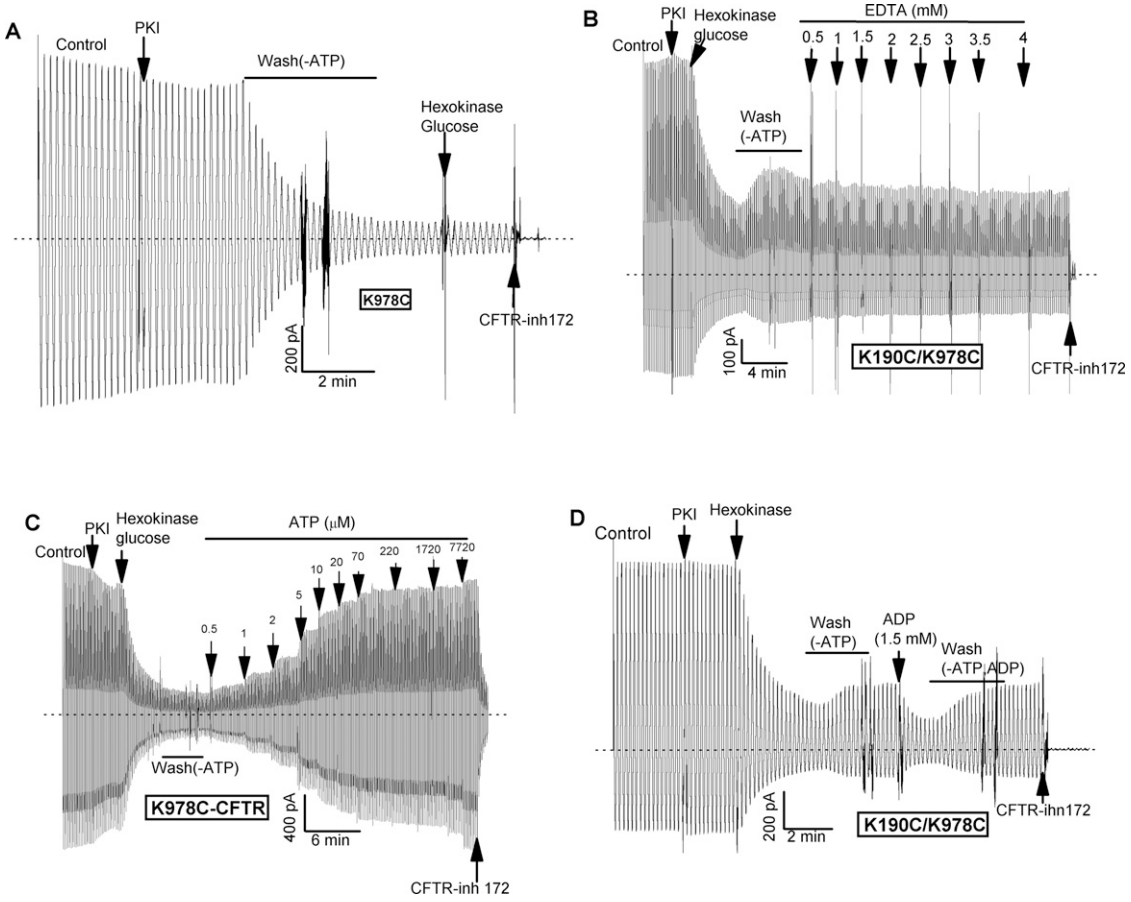

Fig. S1. ATP and ADP sensitivities of loop mutants. (*A* and *B*) Certain loop mutants exhibit stable ATP-independent currents irrespective of how ATP is removed. (*A*) K978C-CFTR: ATP removed by bath perfusion, followed by addition of hexokinase (24 U/mL)/glucose (10 mM). (*B*) ATP was first removed by addition of hexokinase/glucose, followed by bath perfusion with ATP-free solution. EDTA was then added to chelate bath Mg^{2+} (3 mM Mg^{2+} in bath solution), a maneuver known to accelerate ATP unbinding from CFTR (notably, from NBD1 [Aleksandrov L, Aleksandrov A, Riordan JR (2008) Mg^{2+}-dependent ATP occlusion at the first nucleotide-binding domain (NBD1) of CFTR does not require the second (NBD2). *Biochem J* 416:129–136]). (*C*) Representative ATP titration for the K978C constitutive mutant. Current was activated by PKA/ATP, and ATP was then removed by hexokinase/glucose, followed by bath perfusion (conditions described in Fig. 1) before performing the ATP titration. (*D*) ADP reversibly inhibits the constitutive activity of the K190C/K978C-CFTR mutant in the absence of ATP.

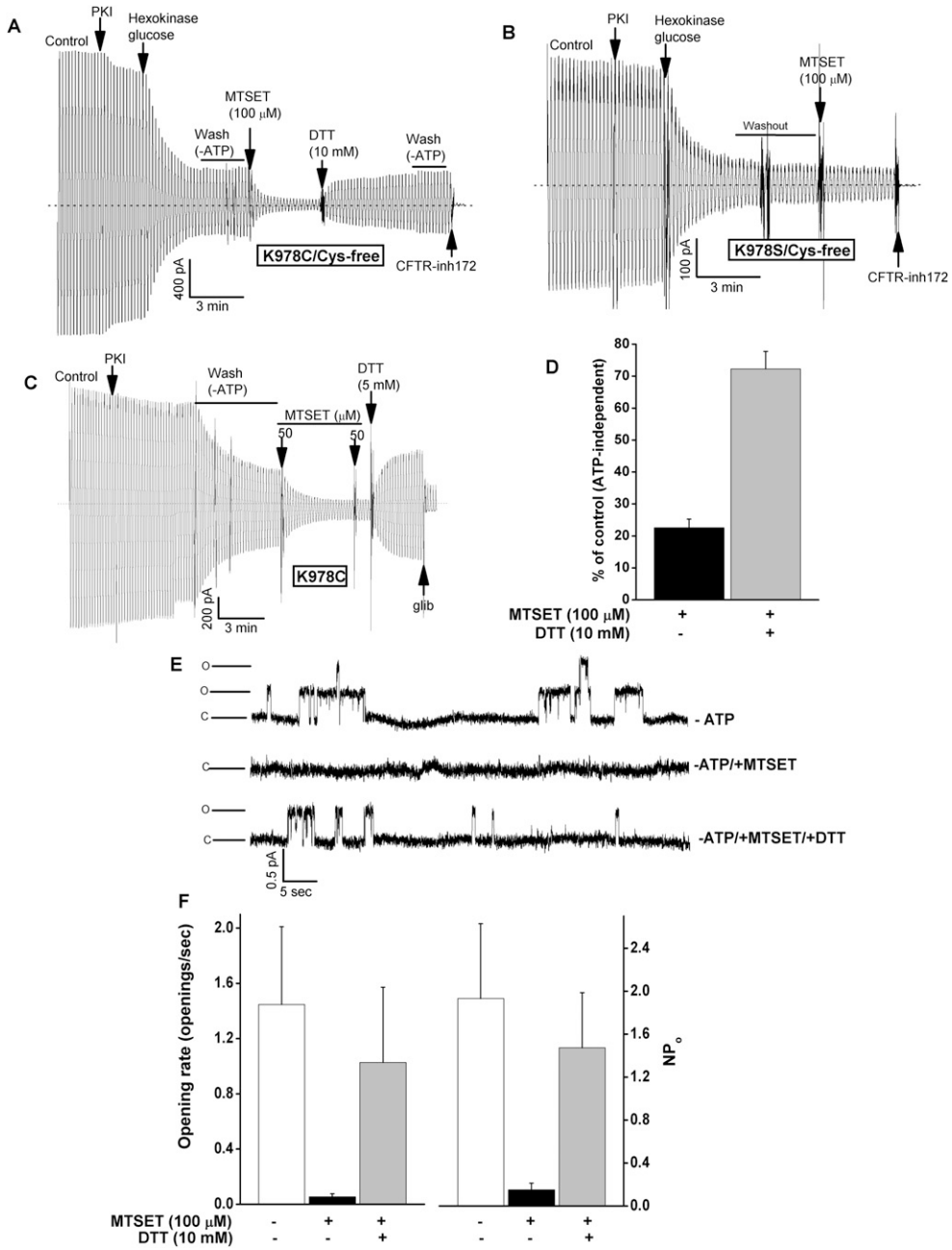

Fig. S2. Accessibility of K978C to thiol modification. (*A*) Positively charged MTSET [Fu J, Kirk KL (2001) Cysteine substitutions reveal dual functions of the amino-terminal tail in cystic fibrosis transmembrane conductance regulator channel gating. *J Biol Chem* 276:35660–35668] reversibly inhibited the ATP-independent current mediated by the K978C mutant (cysteine-free background). (*B*) There was no effect of MTSET on the K978S mutant in the cysteine-free background. (*C*) Similar inhibitory effect of MTSET on the K978C mutant in the WT background (contains native cysteines). (*D*) Mean data (±SEMs) showing degree of MTSET inhibition and DTT recovery for K978C-cysteine-free-CFTR (n = 5). (*E*) Single-channel traces in gap-free recording mode for K978C (cysteine-free background) following ATP removal by hexokinase/glucose addition (+60-mV holding potential; patch obtained using small-tipped pipette). (*Top*) "Control" trace after ATP removal. Note that these channels open and close spontaneously in the absence of ATP. (*Middle*) After addition of 100 μM MTSET. (*Bottom*) After subsequent addition of 10 mM DTT. (*F*) Mean data (±SEMs) showing magnitudes of effects of MTSET and DTT on channel opening rate (openings/seconds per patch) and NP_o (n = 5).

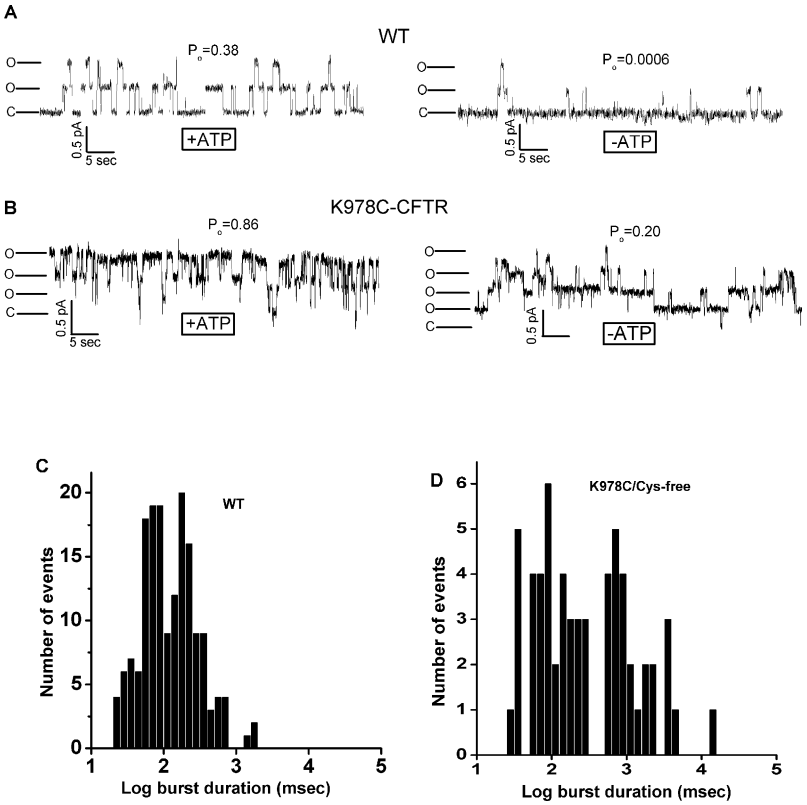

Fig. S3. Multichannel patch records of WT-CFTR and K978C-CFTR channel gating. (*A*) Representative gap-free records of multichannel patches containing WT-CFTR channels in the presence of ATP (*Left*) or after ATP removal by hexokinase/glucose followed by bath perfusion (*Right*) (+60-mV holding potential). Calculated P_os for each patch are indicated above (details of analysis presented in *Methods*). (*B*) Corresponding records for patches containing K978C-CFTR channels. (*C* and *D*) Open time histograms of WT-CFTR and K978C-cysteine-free channels for openings detected after ATP removal. Data were pooled from two and three patches that exhibited single-channel openings, respectively. WT-CFTR openings in the absence of ATP were detected using large-tipped pipettes (2–3 MΩ), and K978C/Cys-free openings in the absence of ATP were detected using smaller tipped pipettes (9–13 MΩ).

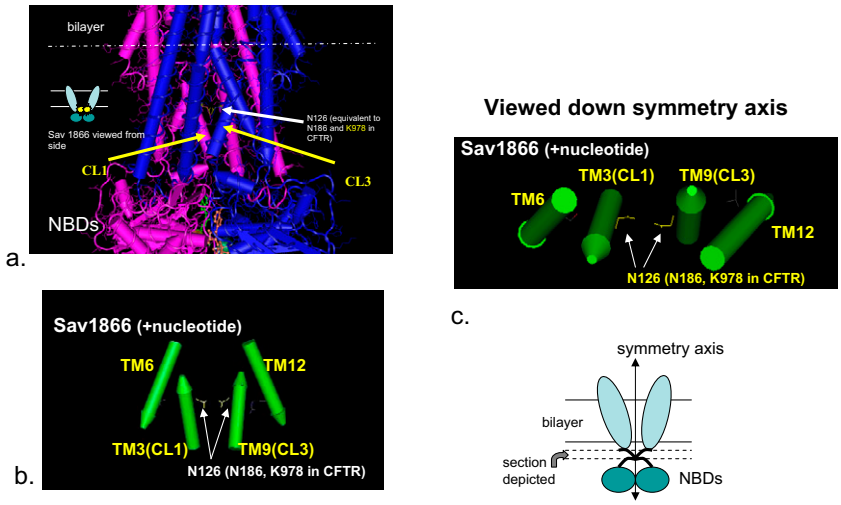

Fig. S4. Cytosolic loops 1 and 3 form an interface along the symmetry axis of the nucleotide-bound Sav1866 structure. (*A*) Side view of AMP-PNP-bound Sav1866 structure with loops 1 and 3 indicated [Dawson RJ, Locher KP (2006) Structure of a bacterial multidrug ABC transporter. *Nature* 443:180–185]. Note that loops 1 and 3 are the cytosolic extensions of TM3 and TM9, respectively. (*B*) Side view of loops 1 and 3 and TM6 and TM12 with other regions omitted for clarity. (*C*) View down symmetry axis.

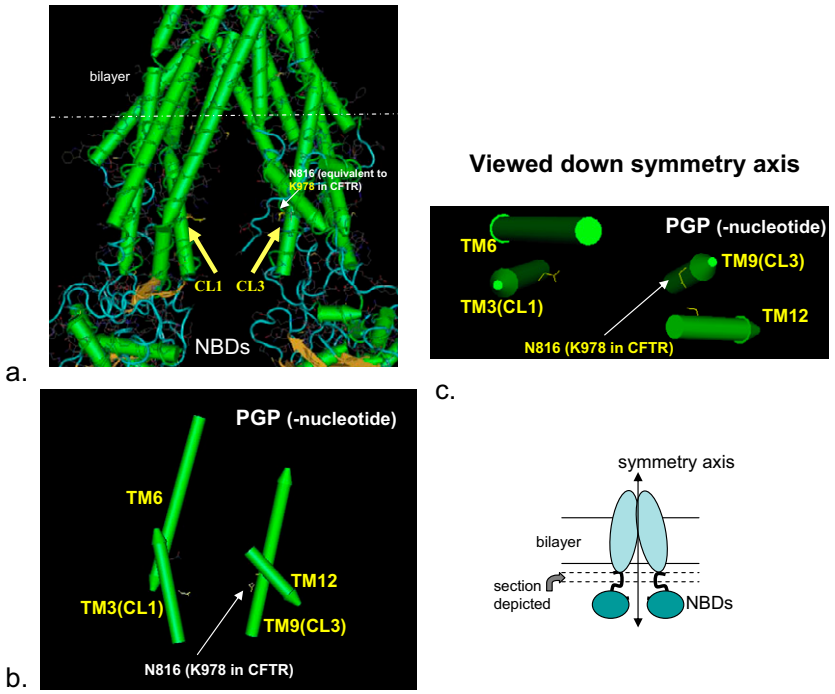

Fig. S5. Orientations of cytosolic loops 1 and 3 in the nucleotide-free P-glycoprotein (PGP) structure. Loops 1 and 3 remain along the symmetry axis but are farther apart compared to the nucleotide-bound Sav1866 structure. Here, loop 3 closely opposes the cytosolic extension of TM12. Conceivably, loop 3 mutations promote constitutive activity by destabilizing the latter interaction [Aller SG, et al. (2009) Structure of P-glycoprotein reveals a molecular basis for poly-specific drug binding. *Science* 323:1718–1722].

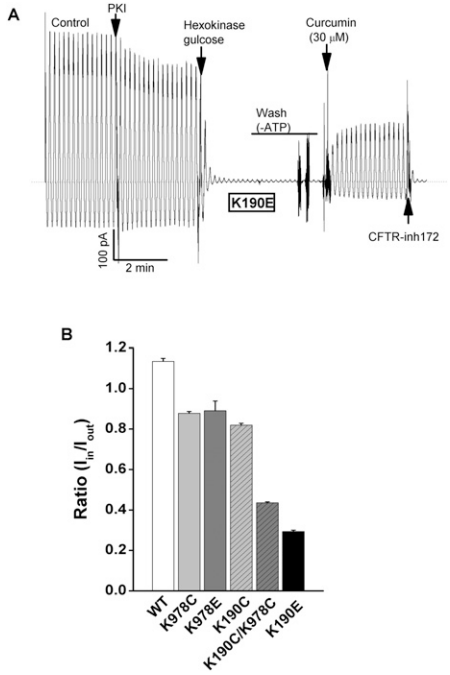

Fig. S6. Current rectification by loop mutants. (*A*) K190E-CFTR current trace showing rectifying current behavior. (*B*) Mean data (±SEMs) showing degree of rectification exhibited by indicated loop mutants (n = 3–19). The stronger rectification of the K190E mutant might be attributable to this position being relatively near the inner pore vestibule.

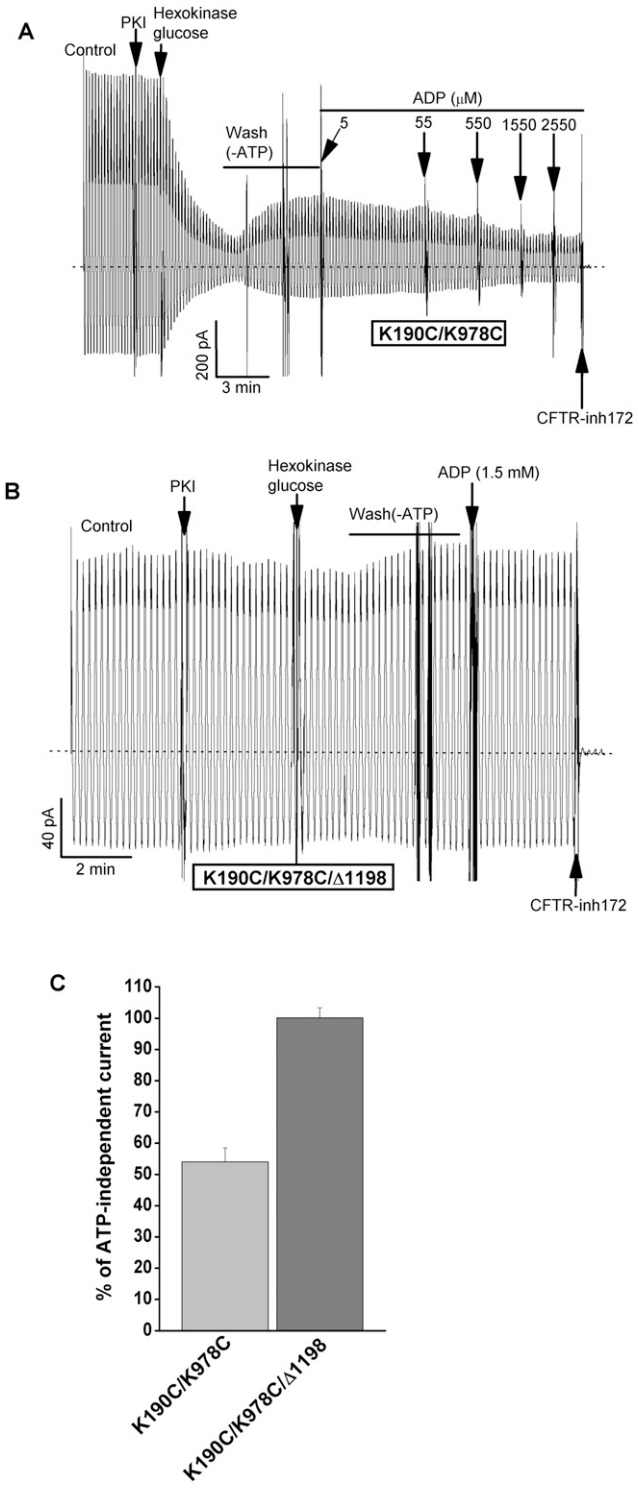

Fig. S7. ADP does not inhibit current by the constitutive loop mutant in the absence of NBD2. (*A*) ADP inhibits ATP-independent current mediated by K190C/K978C-CFTR in a dose-dependent fashion. (*B*) ADP does not inhibit the current mediated by the same loop mutant in a truncation construct lacking NBD2 (Δ1198-CFTR) [Wang W, Bernard K, Li G, Kirk KL (2007) Curcumin opens cystic fibrosis transmembrane conductance regulator channels by a novel mechanism that requires neither ATP binding nor dimerization of the nucleotide-binding domains. *J Biol Chem* 282:4533–4544]. (*C*) Mean inhibition (±SEMs) by 1.5 mM ADP of currents mediated by the indicated constructs (n = 4–6).

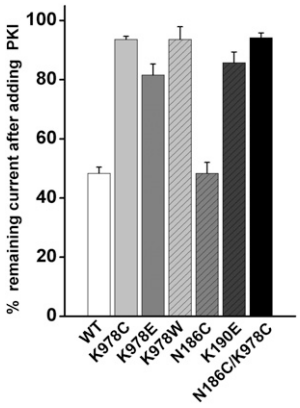

Fig. S8. Most loop 1 and 3 mutants reduce the degree of current inhibition by PKI (conditions described in legend for Fig. 1). Means ± SEMs (n = 4–18).

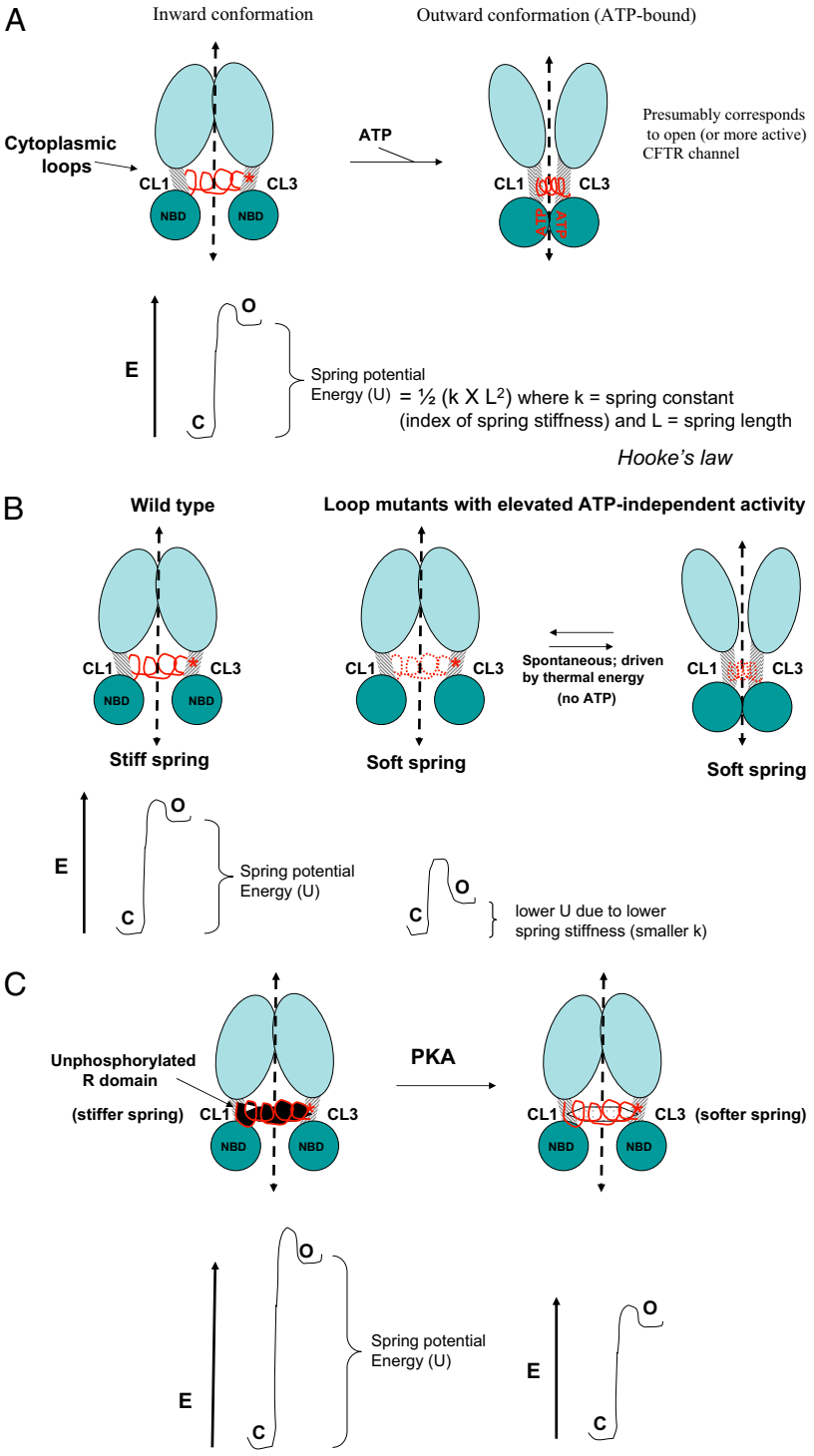

Fig. S9. Cytoplasmic loops as a compression spring. (*A*) Loops are modeled as a simple compression spring whose potential energy and stiffness are given by Hooke's law. The same general concepts would apply if the loops behaved more like a torsion (rotary) spring. (*B*) Certain loop mutations may promote ATP-independent activity by reducing spring stiffness (e.g., by disrupting loop-transmembrane domain interactions that normally stabilize the inactive state of the channel). (*C*) R domain may also regulate spring stiffness by interacting with the loops.